

Research article

## **Prediction of corrosion rate of AZ31B magnesium alloy under salt fog environment in NaCl solution**

*D.Thirumalaikumarasamy\*, K.Shanmugam and V. Balasubramanian*

*Department of Manufacturing Engineering, Faculty of Engineering, Annamalai University, Tamil Nadu, India*

Received 06 December 2012    Revised 20 June 2013    Accepted 26 June 2013

### **Abstract**

Magnesium alloys have gained considerable interest as a material for automotive and aerospace applications due to its low density, high specific strength, and good castability. However, another considerable issue is their corrosion properties. This restricts their practical applications. In this present research, corrosion behavior of the AZ31B magnesium alloy was evaluated by conducting salt fog test in NaCl solution at different chloride ion concentrations, pH values, spraying times, and air pressures. The corrosion morphology observation was carried out by optical microscopy and the corrosion products were analyzed by SEM and XRD analysis. An attempt was also made to develop an empirical relationship to predict the corrosion rate of AZ31B magnesium alloy. Four factors five level central composite rotatable design matrix was used to minimize the number of experimental conditions. Response surface (RSM) methodology was used to develop the relationship. The developed relationship can be effectively used to predict the corrosion rate of AZ31B magnesium alloy at 95% confidence level.

©2013 Usak University all rights reserved.

**Keywords:** *Magnesium alloy, chloride ion concentration, response surface methodology, corrosion rate*

### **1. Introduction**

Magnesium is now becoming the material of choice for many lightweight transport component applications due to its combination of low density and excellent physical and mechanical properties', demonstrated by continued and steady market growth over the past 10 years [1]. In the alloyed form, magnesium is the lightest structural metal and is a potential candidate to replace heavier aluminum or steel components, reducing fuel consumption and harmful emissions in the transport sector [2]. However, the use of magnesium alloys for structural applications has limited success due to their poor corrosion properties [3,4].

The salt spray test is an accelerated corrosion test used to evaluate the relative corrosion resistance of materials exposed to a salt spray or salt fog. The salt spray corrosion test helps to estimate the component's service life. Salt spray testing is popular because it is well standardized and reasonably repeatable. Salt spray tests are widely used in the

\*Corresponding author: Tel: +91-09894319865, Fax: +91-4144-238080/238275

E-mail: [tkumarasamy412@gmail.com](mailto:tkumarasamy412@gmail.com)

DOI: <http://dx.doi.org/10.12748/ujms/20131713>

industrial sector, and on marine, automotive, air craft, and military equipment for the evaluation of the corrosion resistance of parts or finished surfaces.

Corrosion resistance of Mg alloys depends on many factors: (i) environment, (ii) alloy composition and microstructure, and (iii) properties of the film developed in the medium to which they are exposed. Concerning the environment, corrosion resistance of magnesium alloys in chloride containing solutions greatly depends on pH and Cl<sup>-</sup> concentration, with no significant influence of oxygen concentration [5]. In general, magnesium and its alloys dissolve at a very low rate in alkaline or poorly buffered sodium chloride solutions, where the pH can increase, due to the formation of a partially protective layer. On the other hand, chloride ions promote rapid attack in neutral aqueous solutions and even higher in acidic solutions. It is also common to find higher corrosion rates with increasing Cl<sup>-</sup> ion concentration at all pH levels. The corrosion of magnesium alloys in non-oxidizing neutral or alkaline chloride solutions at free corrosion potential typically initiates as irregular pits, which spread laterally and cover the whole surface. However, the mechanism is different from the auto-catalytic pitting experienced by stainless steels [6], since there does not seem to be much tendency for deep pitting, possibly as a result of pH increase and magnesium hydroxide film formation. However, this is not always true, since there is a significant influence of the microstructure on the corrosion mechanism, especially in two-phase magnesium alloys.

The corrosion performance of Mg alloys has evoked a great interest during the last few years. It mainly depends on the film formation and varies with the medium to which the specimen is exposed. However, the poor corrosion resistance of magnesium alloys restricts their potentially vast application. Magnesium alloys are very susceptible to galvanic corrosion, which can result in severe pitting, especially in wet and salty environments [7]. Many investigations have been performed in recent years to understand the corrosion of magnesium alloy in low concentration NaCl solution [8,9]. It is known that the corrosion performance of an alloy is, in general, determined by the chemical composition and distribution of its constituent phases in the microstructure. The main reasons for the poor corrosion resistance of magnesium alloys can be summarized as (1) internal galvanic corrosion induced by second phases or impurities and (2) unstable, quasi-passive hydroxide film corroded on magnesium [10,11].

However, a critical limitation for the extensive use of magnesium alloys is their high susceptibility to corrosion, especially in aggressive environments, which is primarily attributed to the high chemical activity of magnesium and the unstable passive film on the surface of these alloys [12]. Many researchers have addressed the influence of various corrosive environments on the corrosion behavior of pure magnesium and/or magnesium alloys for the understanding of environmental factors controlling corrosion [13,14]. It is well known that the corrosion of magnesium/aluminum (Al) alloys in the media greatly depends on the aluminum content, microstructure, and environment, including pH and chloride ion concentration [15].

Merino *et al.* [16] have reported the corrosion attack of Mg, AZ31, AZ80 and AZ91D materials under the salt fog test increased with increasing temperature and Cl<sup>-</sup> concentration. Individual pitting characteristics, including pit surface area and pit volume, were greater for the salt spray surfaces. Martin *et al.* [17] examined the comparison of corrosion pitting under immersion and salt-spray environments on an as-cast AE44 magnesium alloy and reported that the two environments show similar trends with respect to weight loss and thickness loss, although the immersion environment induces greater amounts of weight loss of magnesium. Pardo *et al.* [18] studied the corrosion behavior of silicon-carbide-particle reinforced AZ92 magnesium alloy. They

found that the severe corrosion in salt fog environment with formation of an uneven, cracked and low protective corrosion layer mainly consisting of  $Mg(OH)_2$ . Pathak *et al.* [19] investigated the dual corrosion performance of magnesium-rich primer for aluminum alloys under salt spray test (ASTM B117) and natural exposure. They identified that the surface of magnesium pigment formed magnesium hydroxide surfaces in salt spray test and magnesium carbonate coated surfaces upon field exposure. Ming-Chun Zhao *et al.* [20] investigated the exploratory study of the corrosion of Mg alloys during interrupted salt spray testing and they found that the  $Mg(OH)_2$  surface film on Mg alloys is probably formed by a precipitation reaction when the  $Mg^{2+}$  ion concentration at the corroding surface exceeds the solubility limit.

From the literature review [16-20], it is understood that most of the published information on corrosion behavior of Mg alloys were focused on general corrosion and pitting corrosion of magnesium alloys. Moreover, there is no literature available related to prediction of corrosion rate of magnesium alloys under salt fog environment by means of an empirical relationship incorporating chloride ion concentration, pH value, spraying time, and air pressure. Hence, the present investigation was carried out to develop an empirical relationship to predict the corrosion rate of AZ31B Mg alloy under salt fog conditions. The effect of pH value, chloride ion concentration, spraying time, and air pressure on corrosion behavior of AZ31B magnesium alloy is reported in this paper.

## 2. Experimental Work

The base material, AZ31B magnesium alloy used in this investigation was an extruded cylindrical rod with 16 mm in diameter. The chemical composition of the base material is presented in Table 1. The specimens were cut to the dimensions of 16 mm x 4 mm to evaluate the corrosion rate by salt fog test method. All sides of the surface of the sample were polished using 500#, 800#, 1200#, 1500# grit silicon carbide papers, rubbed against a smooth polishing cloth and then finely polished using 0.5  $\mu m$  diamond paste. They were then degreased ultrasonically in acetone, cleaned with distilled water, and then dried in warm flowing air. The SEM micrograph of AZ31B alloy is shown in Fig. 1 and it basically contains equiaxed grains of 10  $\mu m$  diameter (average) with primary  $\alpha$ -Mg phase and AlMn phase. AlMn locates at the grain boundary and in the matrix.

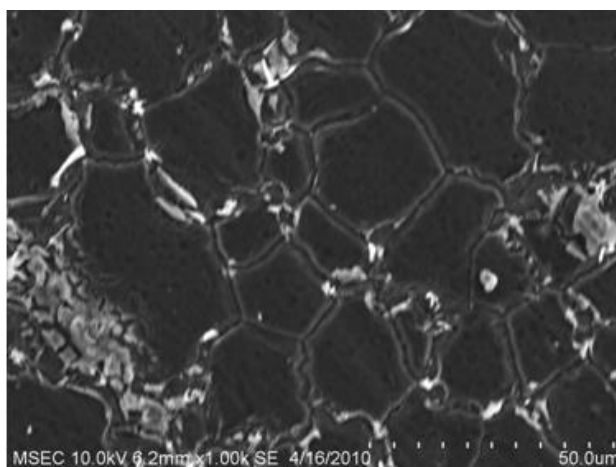


**Fig. 1** SEM micrograph of base alloy (AZ31B Mg alloy)

**Table 1**

Chemical composition (wt %) of AZ31B Mg alloy

Al	Mn	Zn	Mg
3.0	0.20	1.0	Balance

## 2.1. Developing the Experimental Design Matrix

According to Box and Draper [21], the central composite rotatable design (CCRD) is an effective alternative to the factorial design. The CCRD gives almost as much information as a three-level factorial, but requires fewer tests than the full factorial design, and has been shown to be sufficient to describe the majority of corrosion process responses. Hence, in this study, it was decided to use the CCRD to design the experiments. The number of tests required for the CCRD includes the standard  $2^k$  factorial with its origin at the center,  $2k$  points fixed axially at a distance, say  $\alpha$ , from the center to generate the quadratic terms, and replicate the tests at the center; where  $k$  is the number of variables. The axial points are chosen such that they allow rotatability, which ensures that the variance of the model prediction is constant at all points equidistant from the design center. By adding axial points which extend, the design will provide protection against the curvature from twisting. Hence, the design was extended up to  $\pm \alpha$  (axial point). The value of  $\alpha$  is chosen to maintain rotatability. To maintain rotatability, the value of  $\alpha$  depends on the number of experimental runs in the factorial portion of the central composite design, which is given by Eq. 1.

$$\alpha = [\text{number of factorial points}]^{1/4} \quad (1)$$

It can be noted that when  $\alpha > 1$ , each factor is run at five levels ( $-\alpha, -1, 0, +1, +\alpha$ ) instead of the three levels of  $-1, 0$ , and  $+1$ . The reason for running the central composite designs with  $\alpha > 1$  is to have a rotatable design. However, the factorial portion can also be a fractional factorial design of resolution. The center values for the variables were carried out at least six times for the estimation of error, and single runs for each of the other combinations. Replicates of the test at the center are very important as they provide an independent and more uniform estimate of the prediction variance over the entire design.

As the range of individual factor was wide, a central composite rotatable four-factor, five-level factorial design matrix was selected. The experimental design matrix consisting 30 sets of coded condition and comprising a full replication four-factor factorial design of 16 points, 8 star points, and 6 center points was used. Table 2 represents the range of factors considered, and Table 3 shows the 30 sets of coded and actual values used to conduct the experiments. The upper and lower limits of the parameters were coded as  $+2$  and  $-2$ , respectively. Thus, the 30 experimental runs allowed for the estimation of the linear, quadratic, and two-way interactive effects of the variables. The method of designing such a matrix is dealt with elsewhere [22,23]. The coded values for intermediate levels can be calculated from the relationship.

$$X_i = 2 [2X - (X_{max} + X_{min})] / (X_{max} - X_{min}) \quad (2)$$

In Eq. 2,  $X_i$  is the required coded value of a variable  $X$  and  $X$  is any value of the variable from  $X_{min}$  to  $X_{max}$ ,  $X_{min}$  and  $X_{max}$  are the lower and upper level of the variable, respectively.

**Table 2**  
Important factors and their levels

S.No	Factor	Notation	Unit	Levels				
				-2	-1	0	+1	+2
1	pH value	<i>P</i>	-	3	5	7	9	11
2	NaCl	<i>C</i>	(wt. %)	2	3	4	5	6
3	Spraying time	<i>T</i>	Hours(h)	1	2	3	4	5
4	Air pressure	<i>A</i>	kPa	69	104	139	174	209

**Table 3**  
Design matrix and experimental results

Ex. No	Coded values				Original values				Corrosion rate (mm/y)
	P	C	T	A	P (pH)	C (M)	T (hr)	A (kPa)	
1	-1	-1	-1	-1	5	3	2	104	3.25
2	1	-1	-1	-1	9	3	2	104	2.35
3	-1	1	-1	-1	5	5	2	104	4.17
4	1	1	-1	-1	9	5	2	104	3.39
5	-1	-1	1	-1	5	3	2	104	4.11
6	1	-1	1	-1	9	3	2	104	2.17
7	-1	1	1	-1	5	5	2	104	4.73
8	1	1	1	-1	9	5	2	104	2.73
9	-1	-1	-1	1	5	3	4	174	7.81
10	1	-1	-1	1	9	3	4	174	5.96
11	-1	1	-1	1	5	5	4	174	11.32
12	1	1	-1	1	9	5	4	174	6.21
13	-1	-1	1	1	5	3	4	174	2.17
14	1	-1	1	1	9	3	4	174	3.81
15	-1	1	1	1	5	5	4	174	6.60
16	1	1	1	1	9	5	4	174	4.87
17	-2	0	0	0	3	4	3	139	7.90
18	2	0	0	0	11	4	3	139	3.17
19	0	-2	0	0	7	2	3	139	1.37
20	0	2	0	0	7	6	3	139	4.10
21	0	0	-2	0	7	4	1	139	6.69
22	0	0	2	0	7	4	5	139	2.89
23	0	0	0	-2	7	4	3	69	8.32
24	0	0	0	2	7	4	3	209	2.27
25	0	0	0	0	7	4	3	139	5.91
26	0	0	0	0	7	4	3	139	4.81
27	0	0	0	0	7	4	3	139	5.27
28	0	0	0	0	7	4	3	139	4.79
29	0	0	0	0	7	4	3	139	5.03
30	0	0	0	0	7	4	3	139	4.73

**2.2. Recording the Responses**

Solution of NaCl with concentrations of 2 M, 3 M, 4 M, 5 M, and 6 M were prepared. The pH value of the solution was maintained as pH 3, pH 5, pH 7, pH 9, and pH 11 with concentrated HCl and NaOH respectively. The pH value was measured using a digital pH meter. The test method consists of exposing the material to be tested in a salt spray

chamber as per ASTM B 117 standards and evaluating the corrosion tested specimen with the method as per ASTM G1-03 [24,25]. A salt spray chamber was used for this study in conjunction with an air compressor. Basically, the salt spray test procedure involves the spraying of a salt solution onto the samples being tested. This was done inside a temperature controlled chamber. The glass racks were contained in the salt fog chamber (3' high, 3' deep and 5' wide). The samples under test were inserted into the chamber, following which the salt-containing solution was sprayed as a very fine fog mist over the samples. NaCl in tapped water was pumped from a reservoir to spray nozzles. The solution was mixed with humidified compressed air at the nozzle and this compressed air atomized the NaCl solution into a fog at the nozzle. The air pressure was maintained at 69, 104, 139, 174, and 209 kPa respectively. Heaters were maintained at 35°C cabinet temperature. Within the chamber, the samples were rotated frequently so that all samples were exposed uniformly to the salt spray mist. The temperature within the chamber was maintained at a constant level. Since the spray was continuous, the samples were continuously wet, and therefore, uniformly subjected to corrosion.

The corrosion rates of the AZ31B magnesium alloy were estimated through the weight loss measurement. The original weight ( $w_0$ ) of the specimen was recorded and then the specimen was sprayed with the solution of NaCl for different spraying times of 1, 2, 3, 4 and 5 hours. The corrosion products were removed by immersing the specimens for one minute in a solution prepared by using 50 g chromium trioxide ( $\text{CrO}_3$ ), 2.5 g silver nitrate ( $\text{AgNO}_3$ ), and 5 g barium nitrate ( $\text{Ba}(\text{NO}_3)_2$ ) in 250 ml distilled water. Finally, the specimens were washed with distilled water, dried, and weighed again to obtain the final weight ( $w_1$ ). The weight loss ( $w$ ) can be measured by using the following relation;

$$w = (w_0 - w_1) \quad (3)$$

The corrosion rate of AZ31B magnesium alloy was calculated by using the following equation,

$$\text{Corrosion rate} \left( \frac{\text{mm}}{\text{y}} \right) = \frac{87.6 \times w}{A \times D \times T} \quad (4)$$

where,  $w$  is weight loss (g),  $A$  is surface area of the specimen ( $\text{cm}^2$ ),  $D$  is density of the material ( $1.74 \text{ g/cm}^3$ ) and  $T$  is corrosion time (h).

Microstructural examination of the corroded specimens was carried out using a light optical microscope (Make: MEIJI, Japan; Model: MIL-7100) incorporated with an image analyzing software (Metal Vision). The exposed samples surface was prepared for the micro examination both in the "AS polished" and "AS etched" conditions. Picral+Acetic acid were used as etchant. The corrosion test specimens were polished in disc polishing machine for scratch fewer surfaces and the surface was observed at 200X magnification. Phase analysis of the corroded surfaces were performed on Philips 3121 X-ray diffractometer using  $\text{CuK}\alpha$  radiation which was set at 40 kV and 20 mA for the XRD analysis and the data were recorded in the  $2\theta$  range  $10^\circ$  to  $80^\circ$  in steps of  $2^\circ/\text{min}$ .

### 3. Development of Empirical Relationship

In the present investigation, to correlate the salt spray test parameters and the corrosion rate, a second order quadratic model was developed. The response (corrosion rate) is a function of pH value ( $P$ ), chloride ion concentration ( $C$ ), spraying time ( $T$ ), and air pressure ( $A$ ) and it can be expressed as below:

$$CR = f\{P, C, T, A\} \tag{5}$$

The second order polynomial (nonlinear regression) equation was used to represent the response surface and it (Y) is given by:

$$Y = b_0 + \sum b_i x_i + \sum b_{ii} x_i^2 + \sum b_{ij} x_i x_j, \tag{6}$$

For three factors, the selected polynomial could be expressed as:

$$CR = b_0 + b_1(P) + b_2(C) + b_3(T) + b_4(A) + b_{12}(PC) + b_{13}(PT) + b_{14}(PA) + b_{23}(CT) + b_{24}(CA) + b_{34}(TA) + b_{11}(P^2) + b_{22}(C^2) + b_{33}(T^2) + b_{44}(A^2) \tag{7}$$

Where  $b_0$  is the average of responses (corrosion rate) and  $b_1, b_2, b_3, \dots, b_{44}$  are the coefficients that depend on their respective main and interaction factors, which were calculated using the expression given below as:

$$B_i = \sum(X_i Y_i) / n \tag{8}$$

where 'i' varies from 1 to n, in which  $X_i$  is the corresponding coded value of a factor and  $Y_i$  is the corresponding response output value (corrosion rate) obtained from the experiment and 'n' is the total number of combinations considered. All the coefficients were obtained applying central composite face centered design using the design expert statistical software package. After determining the significant coefficients (at 95% confidence level), the final relationship was developed using only these coefficients. The final empirical relationship obtained by the above procedure to estimate the corrosion rate of AZ31B magnesium alloy is given below as:

$$CR = \{5.08 - 0.92 (P) + 0.74 (C) - 0.87 (T) + 1.40 (A) - 0.41 (PC) + 0.28 (PT) - 0.09 (PA) + 0.05 (CT) + 0.38 (CA) - 0.90 (TA) + 0.13 (P^2) - 0.56 (C^2) - 0.05 (T^2) + 0.07 (A^2)\} \text{ mm/y} \tag{9}$$

The adequacy of the developed model is tested using the analysis of variance technique (ANOVA). As per this technique, if the calculated value of the *F*-ratio of the developed model is less than the standard *F*-ratio (from *F*-table) value at a desired level of confidence (say 95%), then the model is said to be adequate within the confidence limit. ANOVA test results are presented in Table 4 for the model. From the Table, it is understood that the developed mathematical model is found to be adequate at 95% confidence level. The value of probability > *F* in Table 4 for the model is less than 0.0500, which indicates that the model is significant. In the same way, the terms of *P, C, T, A, TA,* and *C<sup>2</sup>* were found to be significant at a 95 % confidence interval. Lack of fit is insignificant and therefore indicates that the model fits well with the experimental data [26]. Our ratio of 67.394 indicates an adequate signal. The actual value is compared with predicted value as shown in Fig.2. All of these observations indicate the excellent adequacy of the developed empirical relationship and suitability of the regression model.

**Table 4**  
ANOVA test results

Source	Sum of Squares	df	Mean Square	F Value	P-value Prob > F	
Model	129.480	14	9.248	14.150	<0.0001	Sig.
<i>P</i>	20.370	1	20.370	78.990	< 0.0001	
<i>C</i>	13.300	1	13.300	18.920	0.0006	
<i>T</i>	18.170	1	18.170	25.850	0.0001	
<i>A</i>	47.530	1	47.530	67.620	< 0.0001	
<i>PC</i>	2.694	1	2.694	3.833	0.0691	
<i>PT</i>	1.331	1	1.331	1.894	0.1888	
<i>PA</i>	0.130	1	0.130	0.185	0.6729	
<i>CT</i>	0.055	1	0.055	0.079	0.7821	
<i>CA</i>	2.329	1	2.329	3.314	0.0887	
<i>TA</i>	13.010	1	13.010	18.510	0.0006	
<i>P</i> <sup>2</sup>	0.494	1	0.494	0.704	0.4146	
<i>C</i> <sup>2</sup>	8.773	1	8.773	12.480	0.0030	
<i>T</i> <sup>2</sup>	0.074	1	0.074	0.106	0.7489	
<i>A</i> <sup>2</sup>	0.151	1	0.151	0.216	0.6487	
Residual	10.540	15	0.702			
Lack of Fit	9.534	10	0.953	4.732	0.1501	Not Sig.
Pure Error	1.007	5	0.201			
Cor Total	140.020	29				
Std. dev.	0.838	<b>R-squared</b>		0.9976		
Mean	4.757	<b>Adj R-squared</b>		0.9852		
C.V.%	17.610	<b>Pre R-squared</b>		0.9796		
PRESS	56.370	<b>Adeq precision</b>		67.3940		

df: degrees of freedom, CV: coefficient of variation, F: Fisher ratio, p: probability

### 3.1. Validation of the Developed Models

To validate the developed model, three confirmation experiments were carried out with the process parameters chosen randomly close the range of experimental parameters. For the actual responses the average of three measurements was calculated. Table 5 summarizes the experimental condition, the average actual experimental values, the predicted values and the percentage error. The deviation of the predicted values from the actual experimental results is within  $\pm 10\%$ , which shows that the developed models fit closer to the experimental results.

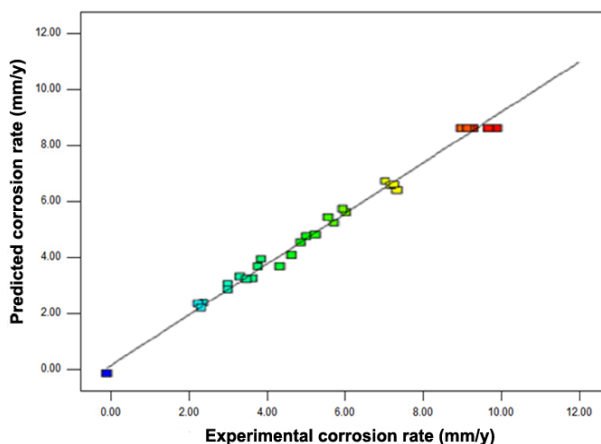


Fig. 2 Correlation graph for response (corrosion rate)

Table 5

Validation of test results

Experimental details					Results	
Input parameters					Responses	
Exp. No	pH	Chloride ion Conc. (M)	Spraying Time (hour)	Air pressure (kPa)	Corrosion rate (mm/yr)	
31	5	3	2	104	Actual	11.926
					Predicted	11.940
					Error %	1.4 %
32	8	5	4	174	Actual	9.150
					Predicted	9.340
					Error %	2.03 %
33	6	4	3	139	Actual	10.130
					Predicted	10.260
					Error %	1.2 %

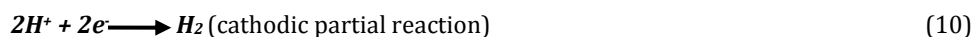
## 4. Discussion

### 4.1. Corrosion Mechanism

The effect of pH of the solutions on the corrosion behavior is in agreement with E-pH diagram of magnesium (Fig. 3) and aluminum. The following points illustrate the mechanisms for all types of corrosion of magnesium alloys.

In acidic media:

Highly acidic solutions are aggressive for both the magnesium and aluminum. In acidic media, probably, anodic dissolution was held. Hydrogen evolution is intimately associated with magnesium dissolution in two separate ways; an electrochemical reaction governed by Eq. 10 balances the magnesium dissolution reaction, Eq. 11



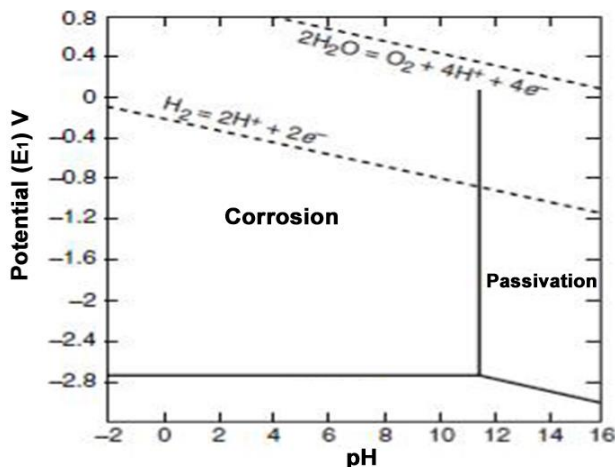
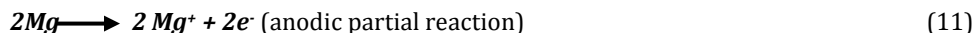
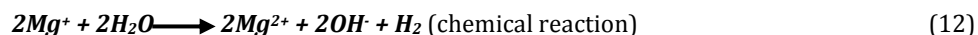


Fig. 3 Potential-pH (Pourbaix diagram) for the system magnesium-water at 25°C

In neutral media:

The corrosion rate decreased with the increase of pH towards neutral region. This may be due to the less aggressiveness of the solution and also as this pH falls in the passive region for aluminum if not for magnesium. In addition, hydrogen is also produced directly in the reaction of  $Mg^{2+}$  with water by Eq. 12.

The overall reaction, Eq. 13, produces one molecule of hydrogen gas for each atom of magnesium dissolved. Furthermore, the overall reaction consumes  $H^{+}$  and produces  $OH^{-}$ , i.e., the pH increases, which favor the formation of a magnesium hydroxide film by the precipitation reaction.



In alkaline media:

In agreement with the above equations, if the pH was above 9, favors the formation of the protective hydroxide film, Eq. 14, (depending upon the concentration of magnesium in solution). The most probable reason is that the cathodic reaction is the liberation of hydrogen as given by Eq. 15. A byproduct of that cathodic reaction is the production of  $OH^{-}$  (or equivalently the consumption of  $H^{+}$ ) with a concomitant increase of the pH and the stabilization of the local magnesium hydroxide film and decrease in corrosion tendency. Thus localized corrosion in magnesium has an inherent tendency to be self-limiting.



The chance development of areas of localized corrosion leads to the undermining and falling out of particles of magnesium, even in the corrosion of pure magnesium. In the present study, the formation of  $Mg(OH)_2$  in corrosion media with starting pH 3 does not mean that these products are stable at this pH value. Since the corrosion attack was

localized in magnesium alloys, a model of pitting corrosion mechanism was shown below, Firstly; the alloy has a protective oxide film in air. When it is sprayed in a sodium chloride aqueous solution, Cl<sup>-</sup> ions will absorb on  $\alpha$  areas bordering on Mg<sub>17</sub>Al<sub>12</sub> particles. If the breakdown potential of the oxide film reaches its free corrosion potential ( $E_{\text{corr}} \sim -1.53\text{V}$  for AZ series Magnesium alloys), then the  $\alpha$ -matrix as an anode, compared to Mg<sub>17</sub>Al<sub>12</sub> particles, starts to dissolve, and a corrosion nucleus may form nearby an Mg<sub>17</sub>Al<sub>12</sub> particle. The nucleus develops a corrosion pit, this may result in Mg(OH)<sub>2</sub> formation and hydrogen evolution according to the chemical reactions

Anodic reaction:



Cathodic reaction:

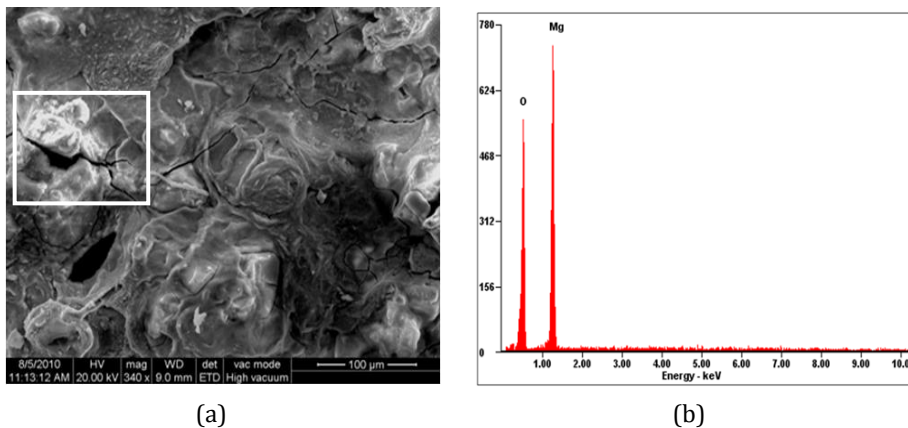


Total reaction:



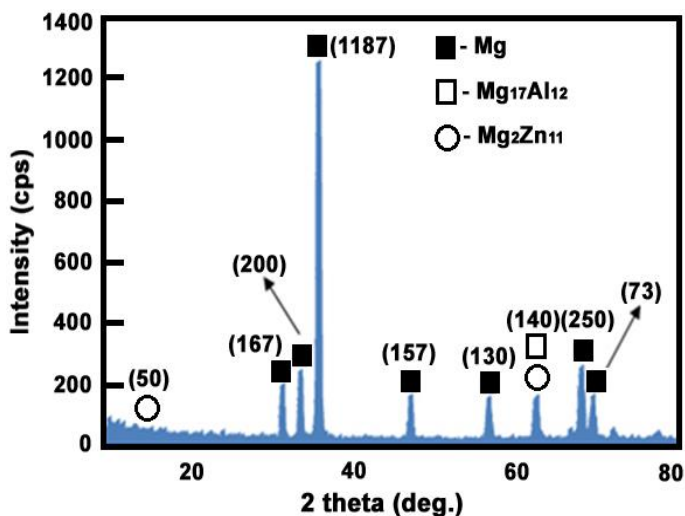
#### 4.2. SEM and XRD Analysis

Fig. 4 shows the SEM EDAX results for the specimens underwent salt spray corrosion tests. Here, the SEM EDAX was represented by the oxygen content of the surface of the specimen. It shows the corrosion products consisting of oxygenated layer mainly Mg(OH)<sub>2</sub>.

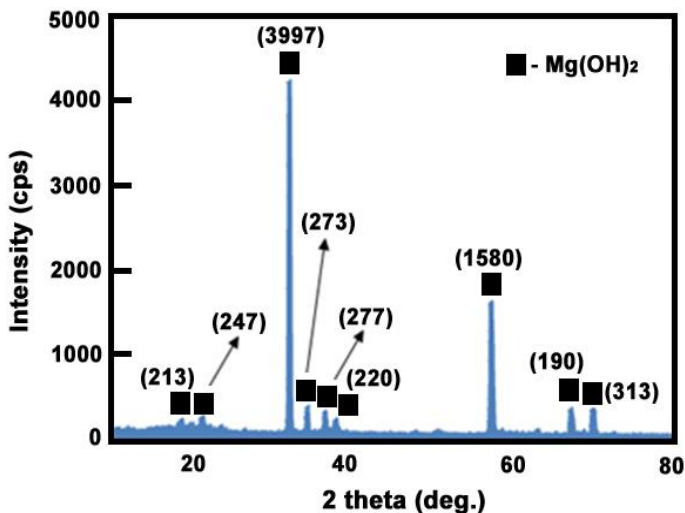


**Fig. 4** SEM (a) and EDAX (b) results of AZ31B magnesium alloy after salt fog test in NaCl solution

Fig. 5a shows the XRD for AZ31, which exhibits on the  $\alpha$ -Mg matrix phase and the results confirm the presence of Al<sub>12</sub>Mg<sub>17</sub> (JCPDS Card No. 73-1148) precipitates along with the traces of Mg<sub>2</sub>Zn<sub>11</sub>. XRD study of the corrosion layer produced after salt fog test in NaCl solution revealed brucite (Mg(OH)<sub>2</sub>) (JCPDS Card No. 86-0441) as the main corrosion product, and its peaks exhibited higher intensity for AZ31 alloy due to the formation of a thicker corrosion layer during the severe attack that the material suffered which is schematically depicted in Fig. 5b. Mg(OH)<sub>2</sub> (brucite) has a hexagonal crystal structure and undergoes easily basal cleavage causing cracking and curling in the film.



(a)



(b)

Fig. 5 XRD Results of (a) AZ31B Mg alloy (before salt fog test) and (b) AZ31B Mg alloy (after salt fog test)

### 4.3. Effect of pH Value on Corrosion Rate

Fig. 6 shows the effect of pH on corrosion morphology of the corrosion test specimen sprayed in 4 M concentration of NaCl for 3 hours and air pressure of 139 kPa with different pH values of pH 3, pH 7 and pH 11. It was seen that, at lower concentration, the surface of the specimen was relatively slightly corroded in neutral and alkaline solutions while severely corroded at all pH values at higher chloride ion concentrations. The corrosion of AZ31B alloy was significantly influenced by pH.

The dissolution of magnesium in aqueous solutions proceeded by the reduction of water to produce magnesium hydroxide Mg (OH)<sub>2</sub> and hydrogen gas (H<sub>2</sub>). The reduction process was primarily water reduction. These reactions are reported to be insensitive to oxygen concentration.



Highly acidic solutions are aggressive towards magnesium, hence a very high corrosion rate. In magnesium-aluminum alloys, a pH above 9 favors the formation of Mg (OH)<sub>2</sub> (depending on the concentration of the medium). This corrosion behavior is consistent with the current understanding that the corrosion behavior of magnesium alloys was governed by the characteristics of its surface film [27]. The surface film on magnesium alloys in aqueous solutions is thought to be mainly Mg (OH)<sub>2</sub>. The Eq. 12 describes the surface film formation, this occurs because Mg<sup>2+</sup> has a low solubility. The influence of pH needs to be taken into account the magnesium E-pH diagram (Pourbaix diagram). However, even though the surface film is not thermodynamically stable at low pH values, the dissolution kinetics may be slow and surface film may be formed provided the dissolution kinetics are slower than the formation kinetics [28].

The microstructure and SEM images of the corroded specimens Figs. 6a and d reveals that at lower pH values, surface of the AZ31B magnesium alloy was completely corroded, corrosion pits almost distributed on the entire surface. Visible corrosion became appreciable as the pH value increased (Figs. 6c and f). In the solution with pH 3, the bubbles overflowed and broke away from the specimen surface. The metallic luster of the specimen surface was also gradually lost, and corrosion became much more severe than in other specimens. Pits were also observed which were suspected to be the sites with the β phase. Mg<sub>17</sub>Al<sub>12</sub> has a higher standard potential and exhibits a more passive behavior over a wide pH range in chloride solutions than either Al or Mg. Due to selective attack along the β phase networks, they were gradually attacked and peel from the surface forming the pits was expected to take place at these sites. It meant that the pH value was one of the major factors of corrosion rate [29].

Fig. 7 represents the effect of pH value on corrosion rate. From this figure, it can be inferred that as the pH value increases, the corrosion rate decreases [30]. At every chloride ion concentration and spraying time, the specimen usually exhibited a decrease in corrosion rate with increase in pH. The highest corrosion rate was observed at pH 3 and at neutral pH, the corrosion rate was remained constant approximately and comparatively low corrosion rate was observed in alkaline solution. It was seen that the influence of pH was more at higher concentration as compared to lower concentration in neutral and alkaline solutions [31].

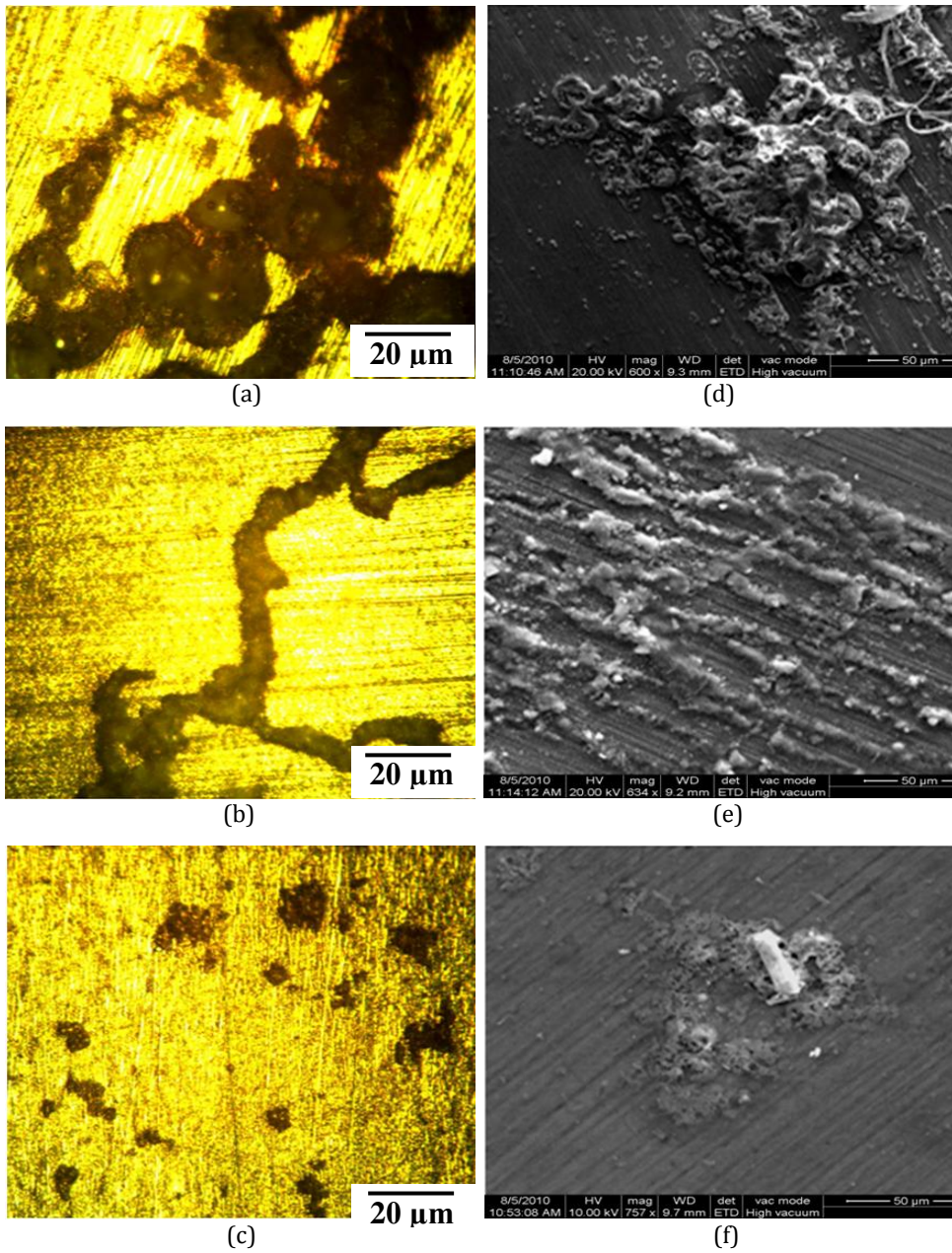


**Fig. 6** Effect of pH value (a,d) pH 3, (b,e) pH 7 and (c,f) pH 11 on corrosion morphology of AZ31B magnesium alloy

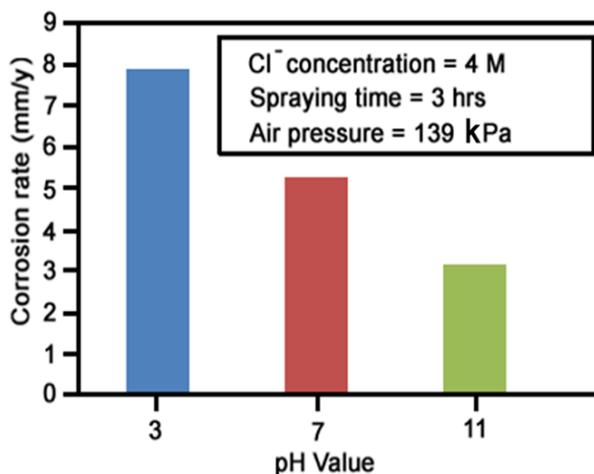


Fig. 7 Effect of pH value on corrosion rate

#### 4.4. Effect of Chloride Ion Concentration on Corrosion Rate

Fig. 8 shows the influence of chloride ion concentration on corrosion morphology of the specimen sprayed in NaCl solution of pH 7 for exposure time 3 hours and air pressure 139 kPa with different chloride ion concentration of 2 M, 4 M and 6 M solutions. It was observed that, the surface of the specimens was covered with corrosion products increase in ratio, with the increase of chloride ion concentration. The corrosion rate of the specimens also increased with increasing chloride ion concentrations. The increase in corrosion rate with the increasing chloride ion concentration was attributed to the participation of chloride ions in the dissolution reaction. Chloride ions are very aggressive to magnesium. The adsorption of chloride ions to oxide covered magnesium surface transforms  $Mg(OH)_2$  to easily soluble  $MgCl_2$  thus destroying the compactness of the corrosion product film and resulting in pitting corrosion [32]. It was considered that the corrosion becomes severe owing to the penetration of hydroxide film by  $Cl^-$  ion and thereby the formation metal hydroxyl chloride complex which governed the following reaction,



This corrosion behavior was consistent with the current understanding that the corrosion behavior of magnesium alloys was governed by a partially protective surface film with the corrosion reaction occurring predominantly at the breaks or imperfections of the partially protective film. The implication is that the fraction of film free surfaces increases with increasing chloride ion concentration. This is consistent with the known tendency of chloride ions to cause with the film breakdown [33].

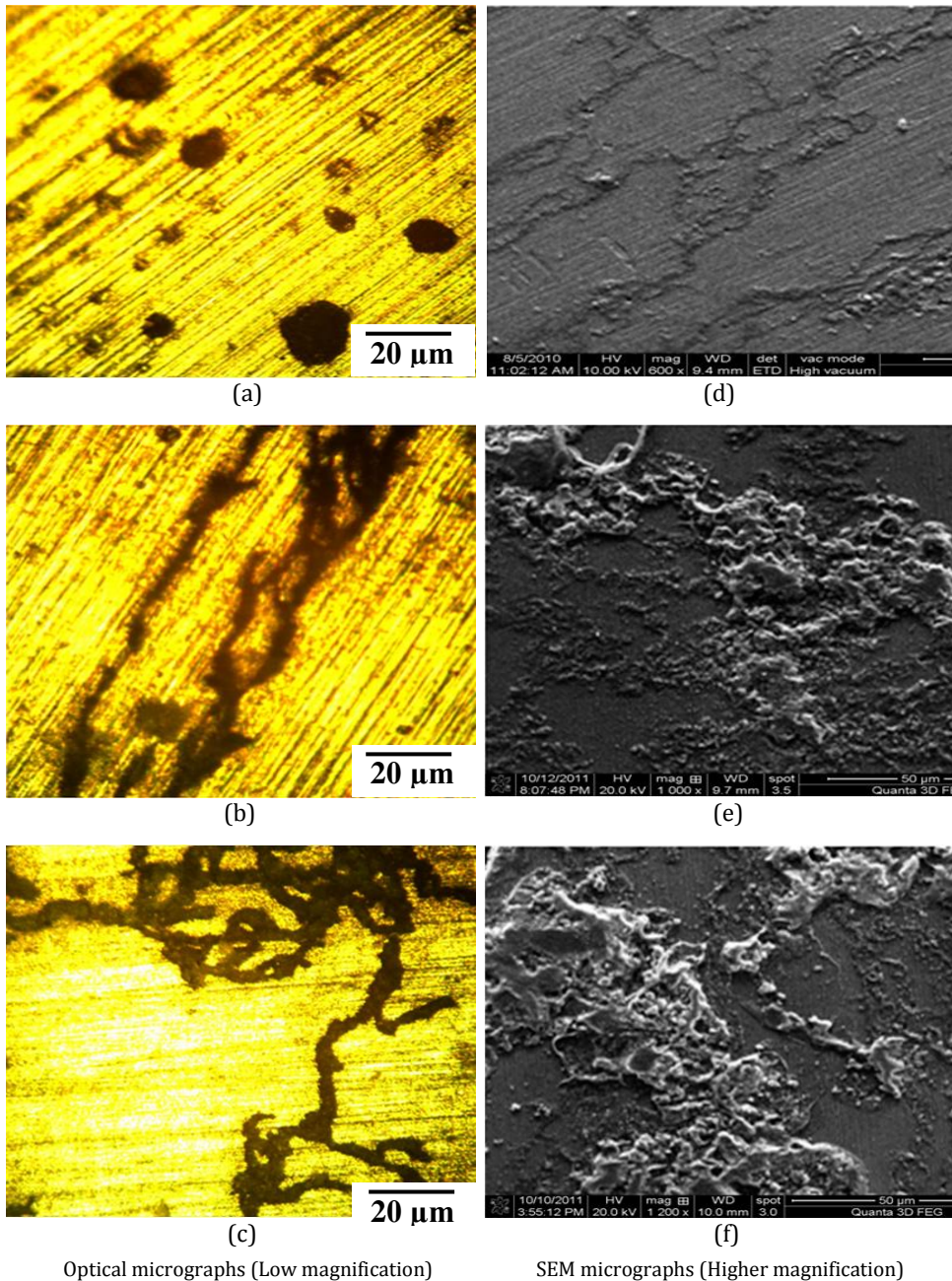


**Fig. 8** Effect of  $\text{Cl}^-$  concentration (a,d) 2M, (b,e) 4M and (c,f) 6M on corrosion morphology of AZ31B magnesium alloy

From the Figs. 8a and 8d, it is also observed that when the chloride ion concentration was low, less corrosion pits were formed on the surface of the AZ31B magnesium alloy. When the chloride ion concentration increased, some obvious pits appeared on the surface of the specimen. The alloy exhibited a rise in corrosion rate with increase in  $\text{Cl}^-$  concentration and thus the change of  $\text{Cl}^-$  concentration affected the corrosion rate much

more in higher concentration solutions than that in lower concentration solutions. When more  $\text{Cl}^-$  in NaCl solution promoted the corrosion, the corrosive intermediate ( $\text{Cl}^-$ ) would be rapidly transferred through the outer layer and reached the substrate of the alloy surface (Figs. 8c and f). Hence, the corrosion rate was increased [34].

Fig. 9 shows the effect of chloride ion concentration on corrosion rate. The graph shows clearly that the corrosion rate was increased with the increase in chloride ion concentration. From the morphological studies, it was observed that, at lower concentration, the surface of the specimen relatively slightly corroded; while severely corrode in the higher concentrations [35].

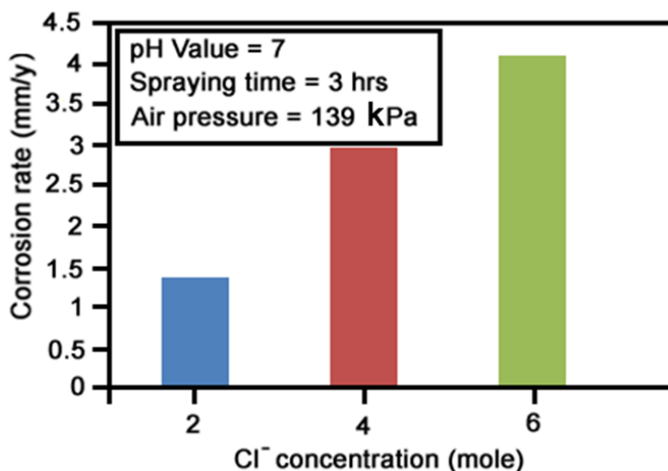
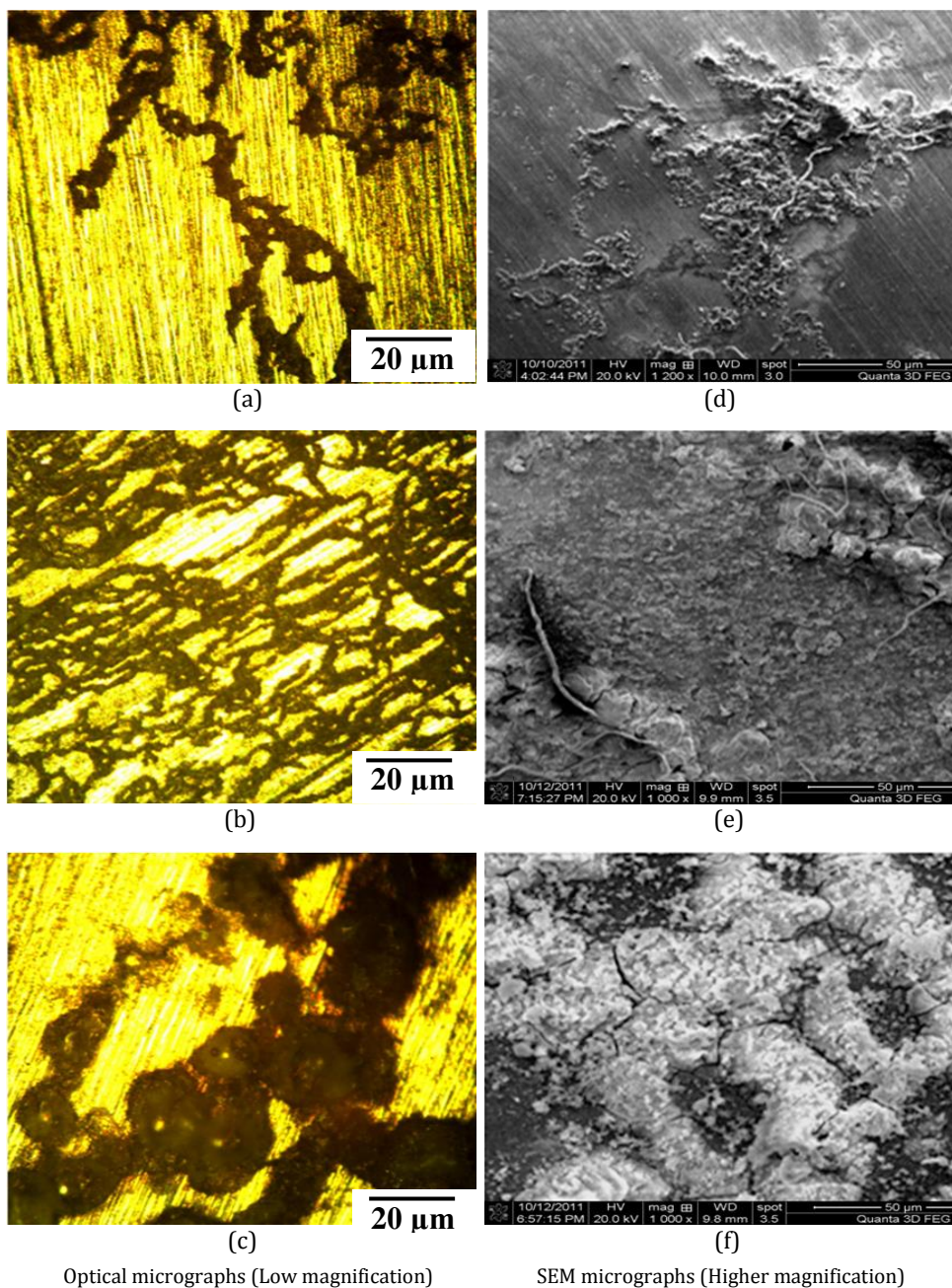


Fig. 9 Effect of  $\text{Cl}^-$  concentration on corrosion rate

#### 4.5. Effect of Spraying Time on Corrosion Rate

Fig. 10 depicts the influence of spraying time on corrosion morphology of the specimen sprayed in NaCl solution of pH 7 for chloride ion concentration 4 M and air pressure 139 kPa with different spraying time of 1, 3 and 5 hours. The corrosion rate decreased with the increase in spraying time. The increase in spraying time enhanced the tendency to form the corrosion products, which accumulated over the surface of the samples. It resulted from the decrease in hydrogen evolution with an increase in spraying time; this is attributed to the corrosion occurring over an increasing fraction of the surface, which is the insoluble corrosion product. The insoluble corrosion product on the surface of the alloy could slow down the corrosion rate [36].

Initial stages of corrosion for AZ31B magnesium alloy in NaCl solution after salt fog test revealed localized corrosion around  $\text{MnAl}_2$  inclusions and  $\beta$ -phase interfaces, which form a galvanic couple with the surrounding mg matrix. AZ31B magnesium alloy after salt fog test in the corrosive medium confirmed the formation of thick corrosion layer with an irregular thickness between 200 and 400  $\mu\text{m}$  and mainly constituted by magnesium oxides and/or hydroxides.



**Fig. 10** Effect of spraying time (a,d) 1 h, (b,e) 3 h and (c,f) 5 h on corrosion behavior of AZ31B magnesium alloy

During the experiment, some black areas appeared initially, these areas became larger and additional similar areas appeared with the increase in spraying time. It was characterized by the observation of localized attack and many upheavals with pitting occurrence. In this case,  $\beta$  phase particles cannot be easily destroyed and, with the increase of corrosion time, the quantity of  $\beta$  phases in the exposed surface would

increase and finally play the role of corrosion barrier. Although, there are some grains of  $\alpha$  phase still being corroded, most of the remaining  $\alpha$  phase grains are protected under the  $\beta$  phase barrier, so the corrosion rate is decreased with the increase of spraying time [37].

As shown in the microstructure and SEM images (Figs. 10a and 10d), at lower spraying times, trench like cavities appeared on the surface of AZ31 specimen. At the higher spraying times, few numbers of corrosion pits were observed on the surface of the material. When the spraying time is more than 3 h, the barrier of the  $\beta$  phase and the adhesion of the corrosion products cause the corrosion weight loss rate to decrease. As a result, the weight loss is greater, and the corrosion weight loss rate is faster. With the prolongation of the spraying time, the corrosion weight loss rate decreases due to the adhesion of the corrosion products to the specimen surface [38]. The film on the specimen surface in the NaCl solution is considerably compacted, which can then effectively prevent further reactions from taking place. Consequently, the growth rate of the film remains slow and forms shallower corrosion dents. It is clear from the Figs. 10c and 10f localized corrosion associated with dense pitted areas showing lot of cracks on the surface of corrosion film for the all specimens tested.

Fig. 11 shows the graph represents the effect of spraying time on corrosion rate. From the Fig, 11, it can be seen that the corrosion rate was decreased with the increase in spraying time. It results that there was an increase in hydrogen evolution with the increasing spraying time, which tends to increase the concentration of  $\text{OH}^-$  ions strengthening the surface from corrosion causing further. Thus the corrosion rate decreased with the increase in spraying time.

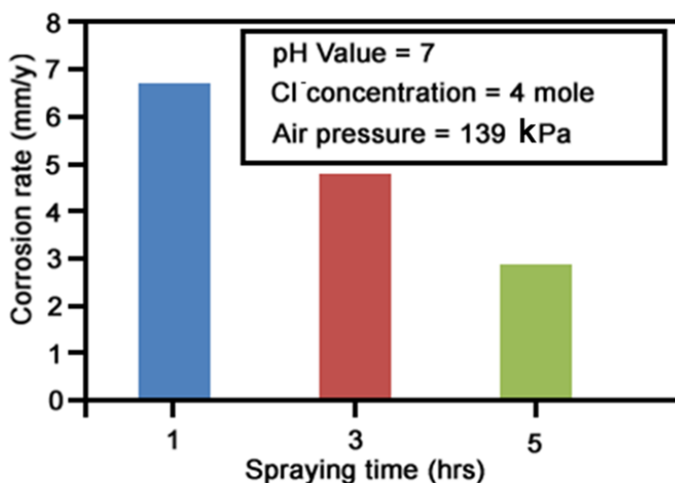
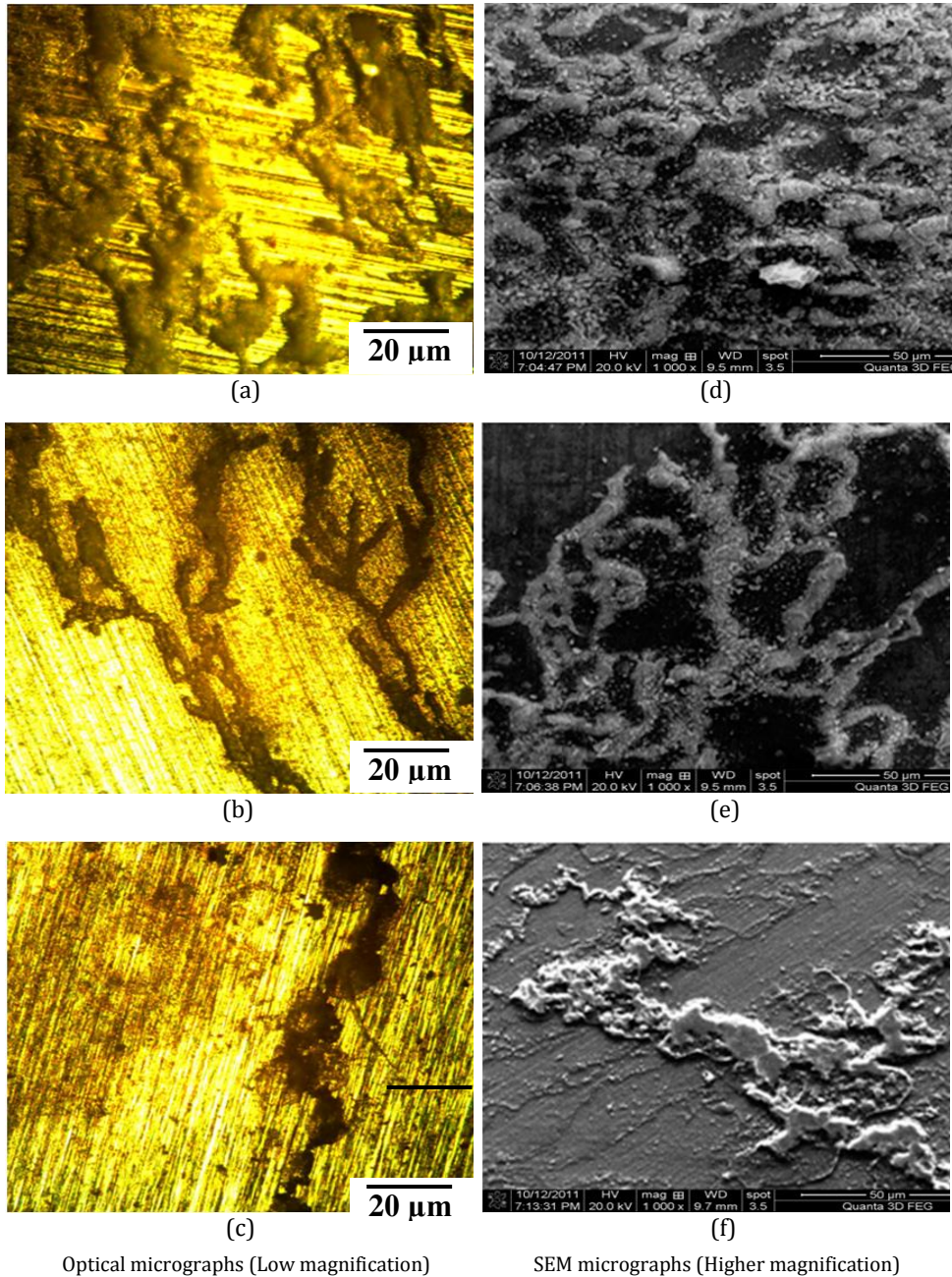


Fig. 11 Effect of spraying time on corrosion rate

#### 4.6. Effect of Air Pressure on Corrosion Rate

Fig. 12 depicts the influence of air pressure on corrosion morphology of the specimen sprayed in NaCl solution of pH 7 for chloride ion concentration 4 M and spraying time 3 hours with different air pressure of 69, 139 and 209 kPa. At low air pressure, more number of pits was formed and pits connected with each other which reflect the propagation/development process of the pitting corrosion. The film formed in the NaCl

solution was uneven, including some cracks, which were wide and deep and distributed irregularly. This indicates that localized corrosion had happened [39]. A passive film constituted of magnesium oxide may exist in the corroded region. The protection of this film baffles the process of the pitting corrosion to some extent.



**Fig. 12** Effect of air pressure (a,d) 69 kPa h, (b,e) 139 kPa and (c,f) 209 kPa on corrosion behavior of AZ31B magnesium alloy

For shorter air pressure the passive film is damaged by attack of chloride ions and the corrosion products are saturated gradually by solution and become expanding. This means the protection of passive film, as well as corrosion products, to magnesium alloy is weakened a lot. Meanwhile, with the dissolution and departure of the products from the base, fresh region of electrode with more vigor is exposed to corrosive medium, which will speed up the pitting corrosion. With the air pressure increasing, there is only one pit on the surface of the electrode, and the pit develops into the base gradually. The electrolyte solutions did not become more susceptible to corrosion. The fast localized corrosion process such as pitting which may correspond to the slow diffusion process of mass or charge around the active corrosion points due to corrosion products. At all concentrations, the materials usually manifested a decrease in corrosion rate with increase in air pressure [40,41].

Figs. 12a and 12d reveals the, at lower air pressure the specimen was damaged severely in a localized region and formed bumped corrosion products in it. It is obvious that the stacked corrosion products have high pitting corrosion, and thus provide nearly no protection against further corrosion. However, at higher air pressure the surface did not suffer severe attack and only the sites with severe corrosion as shown in Figs. 12c and 12f.

Fig. 13 presents the influence of air pressure on corrosion rate. From this figure, it can be inferred that the air pressure has an inversely proportional relationship with the corrosion rate. The numbers of pits were more in the specimens when it is sprayed with the solution of low air pressure as can be observed in Fig. 12. Hence the corrosion rate increases with the decrease in air pressure.

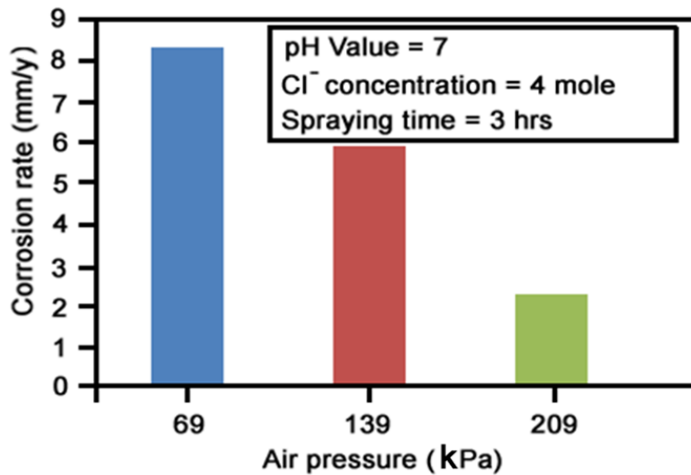


Fig. 13 Effect of air pressure on corrosion rate

## 6. Conclusions

- Empirical relationship was developed to predict the corrosion rate of AZ31B magnesium alloy at a 95% confidence level. The relationship was developed by incorporating the effect of pH value, chloride ion concentration, spraying time and air pressure.

- The AZ31B magnesium alloy exhibited an increment in the corrosion resistance with the increase in pH. The corrosion rate was higher at the acidic media than at the alkaline and neutral media with same concentrations and spraying time. In the salt spray corrosion test, the pH remains constant, as the recycling of the test solution is avoided for further spraying on the test specimens.
- The increase in corrosion rate with increasing chloride ion concentration was attributed to the participation of chloride ions in the dissolution reaction. Chloride ions were very aggressive towards magnesium. The adsorption of chloride ions to oxide covered on magnesium surface transforms  $Mg(OH)_2$  to easily soluble  $MgCl_2$ . There is no variation in the rising rate, because of the formation of magnesium chloride ( $MgCl_2$ ), which is highly soluble. Thus, the corrosion rate increases with the increase in the chloride ion concentration.
- The corrosion rate was decreased with increase in spraying time. The corrosion rate decreased with an increase in spraying time, which implied that the initial corrosion product impeded the passage of corrosion medium and provided protection for metal substrates. The increment in exposure time favors the formation of a protective layer  $Mg(OH)_2$ , which retards the corrosion.
- With the increase in air pressure, the corrosion rate decreases. The increase in air pressure enhanced the tendency to form the corrosion products, which accumulated over the surface of the samples. These corrosion products which in turn depressed the corrosion rate due to the passivation in the spraying.

## Acknowledgements

The authors wish to express their sincere thanks to Mr.R.Selvendiran, Technical Assistant, CEMAJOR, Annamalai University for his help in carrying out this investigation.

## References

1. Pardo A, Merino MC, Merino S, Lopez MD, VIEJO F and Carboneras M. Corrosion behavior of magnesium/aluminium alloys in 3.5 wt. % NaCl. *Journal of Corrosion Science*, 2008; 50: 823 – 834.
2. Tunold R, Holtan H, Berge MH, Lasson A and Hansen RS. The corrosion of magnesium in aqueous solution containing chloride ions. *Journal of Corrosion Science*, 1977; 17: 353 – 365.
3. Ghali E, Dietzel W and Kainer K. General and localized corrosion of magnesium alloys: a critical review, *Journal of Materials Engineering and Performance*, 13: 7 – 23.
4. Nwaogu UC, Blawert C, Scharnagl N, Dietzel W and Kainer KU. Influence of inorganic acid pickling on the corrosion resistance of magnesium alloy AZ31 sheet. *Journal of Corrosion Science*, 2009; 51: 2544 – 2556.
5. Hara N, Kobayashi Y, Kagaya D and Akao N. Formation and breakdown of surface film on magnesium and its alloy in aqueous solutions. *Journal of Corrosion Science*, 2007; 49: 166 – 175.
6. Makar GL and Kruger J. Corrosion of Magnesium. *International Journal of Materials Review*, 1993; 38: 138 – 153.
7. Makar GL and Kruger J. Corrosion studies of rapidly solidified magnesium alloys. *Journal of Electrochemical Society*, 1990; 137: 414 – 421.

8. Jia JX, Song GL and Atrens A. Influence of geometry on galvanic corrosion of AZ91D coupled to steel *Journal of Corrosion Science*, 2006; 48: 2133 – 2153.
9. Shi Z, Song G and Atrens A. The corrosion performance of anodized magnesium alloys. *Journal of Corrosion Science*, 2006; 48: 3531 – 3546.
10. Song G, Hapugoda S and St. John D. Degradation of the surface appearance of magnesium and its alloys in simulated atmospheric environments. *Journal of Corrosion Science*, 2007; 49: 1245 – 1265.
11. Neil WC, Forsyth M, Howlett PC, Hutchinson CR and Hinton BRW. Corrosion of magnesium alloy ZE41 – The role of microstructural features, *Journal of Corrosion Science*, 2009; 51: 387 – 394.
12. Raman RKS. The role of microstructure in localized corrosion of magnesium alloys, *Metallurgical and Materials Transactions A*, 2004; 35: 2527 – 2533.
13. Zeng RC, Zhang J, Huang WJ, Dietzel W, Kainer KU, Blawert C and Andwei KE. Review of studies on corrosion of magnesium alloys. *Transactions of Nonferrous Metal Society of China*, 2006; 16: 763 – 771.
14. Song GL, Johannesson B, Hapugoda S and St. John D. Galvanic corrosion of magnesium alloy AZ91D in contact with aluminium alloy, steel and zinc. *Journal of Corrosion Science*, 2004; 46: 955 – 977.
15. Pardo A, Merino MC, Coy AE, Viejo F, Arrabal R and Feliu Jr S. Influence of microstructure and composition on the corrosion behavior of Mg/Al alloys in chloride media. *Electrochimica Acta*, 2008; 53: 7890 – 7902.
16. Merino MC, Pardo A, Arrabal R, Merino S, Casajus P and Mohedano M. Influence of chloride ion concentration and temperature on the corrosion of Mg–Al alloys in salt fog. *Journal of Corrosion Science*, 2010; 52: 1696 – 1704.
17. Holly JM, Horstemeyer MF and Paul WT. Comparison of corrosion pitting under immersion and salt-spray environments on an as-cast AE44 magnesium alloy. *Journal of Corrosion Science*, 2010; 52: 3624 – 3638.
18. Pardo A, Merino S, Merino MC, Barroso I, Mohedano M, Arrabal R and Viejo F. Corrosion behaviour of silicon–carbide-particle reinforced AZ92 magnesium alloy. *Journal of Corrosion Science*, 2009; 51: 841–849.
19. Pathak SS, Blanton MD, Mendon SK and Rawlins JW. Investigation on dual corrosion performance of magnesium-rich primer for aluminum alloys under salt spray test (ASTM B117) and natural exposure. *Journal of Corrosion Science*, 2010; 52: 1453 – 1463.
20. Box GEP and Draper NR. *Empirical Model Building and Response Surfaces*, John Wiley and Sons, New York, 1987.
21. Zhao MC, Schmutz P, Brunner S, Liu M, Song GL and Atrens A. An exploratory study of the corrosion of Mg alloys during interrupted salt spray testing, *Journal of Corrosion Science*, 2009; 51:1277 – 1292.
22. Khuri AI and Cornell JA. *Response Surfaces; Design and Analysis*, Marcel Dekker Ltd, New York, 1996.
23. Miller RG, Freund JE and Johnson DE. *Probability and Statistics for Engineers*, Prentice of Hall of India Pvt Ltd, New Delhi, 1999.
24. ASTM B 117. *Standard Practice for Operating Salt spray (Fog) apparatus*. American Society for Testing of Materials, 2003.
25. ASTM G1-03. *Standard Practice for Preparing, Cleaning and evaluating Corrosion Test Specimens*. American Society for Testing of Materials, 2003.
26. Montgomery DC. *Design and Analysis of Experiments*, 3, John Wiley, New York, 2001.
27. Inoue H, Sugahara K, Yamamoto A and Tsubakino HT. Corrosion rate of magnesium and its alloys in buffered chloride solution. *Journal of Corrosion Science*, 2002; 44: 603 – 610.

28. Gao L, Zhang C, Zhang M, Huang X and Sheng N. The corrosion of a novel Mg-11Li-3Al-0.5RE alloy in alkaline NaCl solution. *Journal of Alloys & Compounds*; 2007, 468: 285 – 289.
29. Abady GM, Hilal NH, El-Rabiee M and Badawy WA. Effect of Al content on the corrosion behavior of Mg-Al alloys in aqueous solutions of different pH. *Electrochimica Acta*, 2010; 55: 6651 – 6658.
30. Liang J, Bala Srinivasan P, Blawert C and Dietzel W. Influence of pH on the deterioration of plasma electrolytic oxidation coated AM50 magnesium alloy in NaCl solutions. *Journal of Corrosion Science*, 2010; 52: 540 – 547.
31. Hiromoto S, Yamamoto A, Maruyama N, Somekawa H and Mukai T. Influence of pH and flow on the polarisation behaviour of pure magnesium in borate buffer solutions. *Journal of Corrosion Science*, 2008; 50: 3561 – 3568.
32. Hara N, Kobayashi Y, Kagaya D and Akao N. Formation and break down of surface films on magnesium and its alloys in Aqueous solutions. *Journal of Corrosion Science*, 2007; 49: 166 – 175.
33. Pardo A, Merino MC, Coya AE, Viejo F, Arrabal R and Feliu S. Influence of microstructure and composition on the corrosion behaviour of Mg/Al alloys in chloride media. *Electrochimica Acta*, 2008; 53: 7890 – 7902.
34. Lebozec N, Jonsson M and Dominique Thierry. Atmospheric corrosion of magnesium alloys: The influence of temperature, relative humidity, and chloride deposition. *Corrosion*, 2004; 60: 356 – 361.
35. Zhao MC, Liu M, Song GL and Atrens A. Influence of pH and chloride ion concentration on the corrosion of Mg alloy ZE41. *Journal of Corrosion Science*, 2008; 50: 3168 – 3178.
36. Dhanapal A, Rajendra Boopathy S and Balasubramanian V. Developing an empirical relationship to predict the corrosion rate of friction stir welded AZ61A magnesium alloy under salt fog environment. *Materials Design*, 2011; 32: 5066 – 5072.
37. Johnsson M, Persson D and Thierry D. Corrosion product formation during NaCl induced atmospheric corrosion Mg alloy AZ91D. *Journal of Corrosion Science*, 2007; 49: 1540 – 1558.
38. Blawert C, Morales ED, Dietzel W and Kainer KU. Comparison of corrosion properties of squeeze cast and thixocast MgZnRE alloys. *Materials Science Forum*, 2005; 488: 697 – 700.
39. Song G, Atrens A, Wu Z and Zhang B. Corrosion behavior of AZ21, AZ501, and AZ91 in sodium chloride, *Journal of Corrosion Science*, 1998; 40: 1769 – 1791.
40. Song Y, Shan D, Chen R and Han EH. Effect of second phases on the corrosion behavior of wrought Mg-Zn-Y-Zr alloy. *Journal of Corrosion Science*, 2010; 52: 1830 – 1837.
41. Zhang ZM, Xu HY and Li BC. Corrosion properties of plastically deformed AZ80 magnesium alloy. *Transactions of Nonferrous Metal Society of China*, 2010; 20: 697 – 702.